ELSEVIER

Journal of Nuclear Materials 277 (2000) 204–210

journal of nuclear materials

www.elsevier.nl/locate/jnucmat

Micro-structures associated with uraninite alteration

Mostafa Fayek[a,*], Peter Burns[b], Yong-Xiang Guo[c], Rodney C. Ewing[d]

[a] *Department of Earth and Space Science, University of California, 3806 Geology Building, Box 951567, Los Angeles, CA 90095-1567, USA*

[b] *Department of Civil Engineering and Geological Sciences, University of Notre Dame, 166 Fitzpatrick Hall, Notre Dame, IN 46556-0767, USA*

[c] *Department of Earth and Planetary Science, University of New Mexico, Albuquerque, NM 87131-1116, USA*

[d] *Department of Nuclear Engineering and Radiological Sciences, University of Michigan, 2958A Cooley Building, 2355 Bonisteel Boulevard, Ann Arbor, MI 48109-2104, USA*

Received 11 February 1999; accepted 19 July 1999

Abstract

Primary uraninite from the Canadian Proterozoic unconformity-type uranium deposits have exceptionally low, but variable, $\delta^{18}O$ values (-32 to $-15‰$). Although these uranium deposits have been studied extensively, the oxygen isotope systematics in uraninite from these deposits are poorly understood. X-ray powder-diffraction patterns of uraninite with both low and high $\delta^{18}O$ values show that these uraninite samples are consistent with a composition of UO_2 and are texturally similar. Micro-diffraction and lattice images obtained using high-resolution transmission electron microscopy (HRTEM) of uraninite with the lowest $\delta^{18}O$ values show that this uraninite is well crystallized and essentially defect-free. Energy dispersive X-ray spectroscopy of well-crystallized uraninite indicates relatively high Pb contents but low Si and Ca contents. In contrast, micro-diffraction and lattice images of uraninite with $\delta^{18}O$ values near $-18‰$ show that this uraninite is polycrystalline, with micro-diffraction patterns that often show both streaking and concentric patterns. High-resolution images reveal sub-grain formation and rotation, formation of edge dislocations, low-angle grain-boundaries, and bent lattice-fringes. The uraninite is also characterized by relatively high Si and Ca contents and variable Pb contents. This indicates that incipient alteration occurs on a micro-scale as revealed by HRTEM. The sub-grains in this uraninite were preserved either because the annealing process in uraninite was retarded by the Si and Ca impurities, or they were formed during a late alteration event and the uraninite has had little time to anneal.

1. Introduction

Uranium deposits have been used as natural analogues in order to understand the potential migration of uranium and other radionuclides around a spent fuel repository because uraninite and UO_2 (the major constituent of spent fuel) are chemically and structurally similar [1,2]. In this regard, high grade, unconformity-type uranium deposits have been studied extensively, although the extent and process of alteration of uraninite from these deposits is poorly understood.

The unconformity-type uranium deposits of the Athabasca Basin, Canada (Fig. 1) are the highest grade uranium deposits in the world. Although these deposits have been studied extensively, the oxygen isotope systematics of the uraninite and uranium-bearing minerals formed by alteration are poorly understood. In addition, few studies have considered the effects of radiation damage on alteration and isotope fractionation between these radioactive minerals and fluids with which they have subsequently interacted [3,4], although radiation effects are an important consideration in the evaluation of the long-term behavior of spent nuclear fuel.

Three main stages of ore formation are observed in thin section and by back-scattered electron images (BSE;

* Corresponding author.

E-mail addresses: fayek@argon.ess.ucla.edu (M. Fayek), peter.burns.50@nd.edu (P. Burns), yxiang@unm.edu (Y.-X. Guo), rodewing@umich.edu (R.C. Ewing).

0022-3115/00/$ - see front matter
PII: S0022-3115(99)00199-3

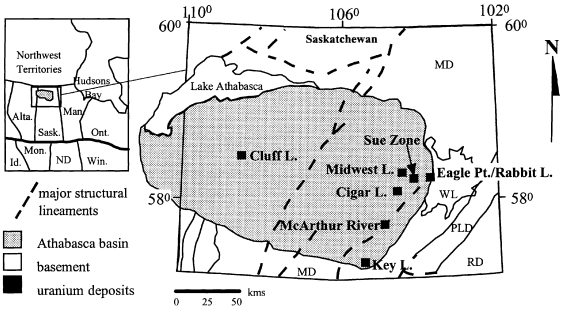

Fig. 1. Map showing the extent of the Athabasca Basin, location of the uranium deposits and major lithostructural domains in the crystalline basement of Saskatchewan (modified from [34]). Abbreviations: MD = Mudjatik Domain; WD = Wollaston Domain; PLD = Peter Lake Domain; RD = Rottenstone Domain; and WL = Wollaston Lake; R = River; L = Lake.

[5]). These are: stages 1 (U1) and 2 (U2) uraninite, and stage 3 uraninite (U3). Stages 1 and 2 uraninite comprise the majority of the ore in these deposits and coincide with two major fluid events at $\sim$ 1500 and 950 Ma, respectively. Stage 3 uraninite occurs in veins and along fractures. Therefore, stages 1 and 2 uraninite are referred to as primary uranium ore. All stages of uranium ore are variably altered to Ca-rich uranyl oxide hydrate minerals and coffinite. This alteration normally occurs on a scale that is detectable only by quantitative electron micro-probe analyses and back-scattered electron imaging of samples [5,6]. Consequently, uraninite has a complex chemistry and structure [6,7].

Uranyl minerals and coffinite have $\delta^{18}O$ values that range from -15 to 0‰; whereas, stage 3 uraninite has $\delta^{18}O$ values that range from -10 to -3.8‰. There is a positive correlation between $\delta^{18}O$ values and SiO_2 and CaO contents of uraninite, uranyl minerals, and coffinite [6], as is expected from the incorporation of relatively $\delta^{18}O$-rich SiO_2 and CaO during formation or alteration of uranium minerals [8]. However, relatively unaltered stages 1 and 2 uraninite that have similar chemical compositions (i.e., low SiO_2 and CaO contents) have a range of oxygen isotopic compositions from -32 to -15‰ [6,9]. In addition, these exceptionally low $\delta^{18}O$ values of natural uraninite (i.e., -32‰), in conjunction with theoretical uraninite–water fractionation factors proposed by [10] and [11], and experimental fractionation factors [12], indicate that primary uraninite in the Athabasca Basin are not in oxygen isotopic equilibrium with the fluids that precipitated coexisting clay and silicate minerals [6,9]. These fractionation factors indicate that primary uranium minerals would have been in equilibrium with fluids that had a $\delta^{18}O$ value of less than -11‰ at ca. 200°C, the temperature at which the deposits formed [13]. However, the dominant fluids that equilibrated with silicate and clay minerals which are associated with primary uranium mineralization, are saline fluids having $\delta^{18}O$ values of 4 ± 2‰ [9,13]. Therefore, using these fractionation factors in conjunction with the low $\delta^{18}O$ values of ca. -28‰ for primary uraninite form unconformity-type uranium deposits in Canada, indicate that the oxygen isotopic composition of the uraninite was completely overprinted by low-temperature ground water and that the uraninite can exchange oxygen isotopes with fluids resulting in only minor disturbances to their chemical composition and texture. However, these fluids must be reducing because uranium mineral chemistry and solubility are largely functions of fO_2 and uraninite is stable only under very reducing conditions ($fO_2 < 10$ and -25, [14,15]).

In this study, primary uraninite (stages 1 and 2) is examined using high-resolution transmission electron microscopy (HRTEM) to resolve chemical and microstructural differences between primary uraninites with low and high $\delta^{18}O$ values, and to assess whether radiation damage could have had an effect on the $\delta^{18}O$ values. Detailed characterization of uraninite and its alteration products and processes may also provide a better understanding of how the UO_2 in spent nuclear fuel will behave under repository conditions over long periods of time [16].

2. Geological considerations

The Athabasca Basin consists of a sequence of Helikian poly-cyclic, mature, fluvial to marine quartz sandstones collectively referred to as the Athabasca Group [17,18]. These rocks are unconformably overly Aphebian metasedimentary and Archean gneisses of the Wollaston Domain of the Trans-Hudson Orogen [19–22]. Deposition of uranium was the result of mixing between 200°C uraniferous oxidizing basinal brines and reducing basement fluids, along Hudsonian faults which crosscut the unconformity between Helikian Athabasca sandstones and Aphebian basement metasedimentary rocks and Archean gneisses. Deposition occurred during peak diagenesis at $\sim$ 1500, $\sim$ 950, and as late as $\sim$ 300 Ma [6,9,23].

The majority of the high-grade uranium mineralization in these deposits occurs as lenses of massive uraninite, the most common reduced (U^{4+}) uranium-bearing minerals. However, subsequent infiltration of low-temperature meteoric water along reactivated fault zones, which host uranium mineralization, has partially altered uraninite to coffinite and uranyl oxide hydrate minerals, and locally remobilized and degraded many of the original high-grade deposits.

Intense hydrothermal alteration in the sandstone and basement gneisses and metasediments surrounding the uranium deposits is characterized by large haloes of illitized sandstone and local enrichments of K, Mg, Ca, B, U, Ni, Co, As, Cu, and Fe [13,23–25]. Extensive areas of

silicification with dravite, kaolinite and chlorite are associated with some deposits [26].

3. Analytical techniques

Drill-core samples of uraninite were collected from a zone of high-grade uranium mineralization in the Cigar Lake deposit located along the eastern margin of the Athabasca Basin, Canada. These samples were examined for homogeneity and alteration using reflected light microscopy, BSE imaging, quantitative electron microprobe analyses, and oxygen isotope analyses. The purity of the sample was further verified by X-ray diffraction and scanning electron microscopy (SEM). Chemical compositions of the uranium oxides were determined by wavelength dispersive X-ray spectroscopy (WDS) using a fully automated JEOL JXA-8600 X-ray micro analyzer at an operating voltage of 15 keV, a beam diameter of 2 μm, and counting times of 40 s per element. Detection limits of the elements were of the order of 0.1 wt%. Data reduction for the various elements was done by taking into account the matrix corrections between standards and samples and the analytical parameters (i.e., take-off angle and operating voltage) of the electron microprobe.

Oxygen was liberated from the uranium oxide minerals using the BrF_5 technique of [27]. Oxygen isotopic compositions are reported as delta values in units of ‰ (parts per thousand) relative to the standard, Vienna Standard Mean Ocean Water (V-SMOW) such that

$$\delta_A = [(R_A - R_{stnd})/R_{stnd}] \times 10^3,$$

where R_A and R_{stnd} are the absolute ratios of $^{18}O/^{16}O$ in the sample (i.e., uraninite) and the standard (i.e., V-SMOW), respectively. The absolute $^{18}O/^{16}O$ ratio of V-SMOW is 2005.2×10^{-6} [28]. The analyses were measured at the University of Saskatchewan on the Finnigan Mat Delta and 251 gas source mass spectrometers. Replicate analyses for $\delta^{18}O$ are reproducible to ±0.2‰ and, using this technique, the $\delta^{18}O$ value of NBS-28 quartz is 9.6‰.

Samples of relatively unaltered stage 1 uraninite with a $\delta^{18}O$ value of −30‰, stage 2 uraninite with a $\delta^{18}O$ value of −28‰, and stage 2 uraninite with a $\delta^{18}O$ value −18‰ were crushed and powdered. Powders were placed on carbon grids and examined using the JEOL JEM-2010 HRTEM at the University of New Mexico. This instrument has analytical capabilities and has a point-to-point resolution of 0.19 nm.

4. Results

Stages 1 and 2 uraninite have similar X-ray powder-diffraction patterns both of which are consistent with the composition UO_2 (Fig. 2). Selected area diffraction and lattice images obtained using HRTEM of stages 1 and 2 uraninite with $\delta^{18}O$ values near −30‰ show that these samples are well crystallized and essentially defect-free (Figs. 3(a), 4(a)). Energy dispersive spectroscopy (EDS) of these well-crystallized uraninite samples indicate that they have relatively high Pb contents but low Si and Ca contents (Figs. 3(b), 4(b)).

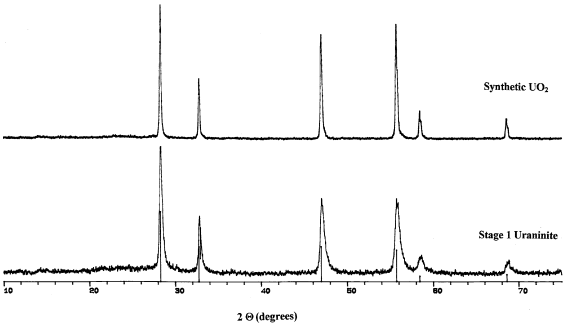

Fig. 2. X-ray powder diffraction patterns of stage 1 uraninite. Also shown for reference is the diffraction pattern of synthetic UO_2 and the major peaks ('stick pattern') for uraninite JCPDS file 41-1422.

In contrast, micro-diffraction and lattice images of stage 2 uraninite with $\delta^{18}O$ values near −18‰ show that this uraninite is polycrystalline (Fig. 5(a)). Micro-diffraction patterns of these uraninite grains often show streaking and concentric diffraction rings. High-resolution images reveal sub-grain formation and rotation, formation of edge dislocations, low angle grain boundaries, and 'bent' lattice fringes (Fig. 5(a)). This uraninite is characterized by relatively high Si and Ca contents and variable Pb contents (Fig. 5(b)).

Bright-field images and EDS analyses of stage 2 uraninite with $\delta^{18}O$ values near −18‰ show that these crystals are structurally complex and chemically heterogeneous (Fig. 6). Regions within a crystal with relatively high Si and Ca contents but depleted in Pb show mottled diffraction contrast (Fig. 6(a)). However, regions with low Si and Ca contents but high Pb content show spheroidal dark patches that are enriched in Pb and U (Fig. 6(b)). In contrast, bright-field images of stages 1 and 2 uraninite with $\delta^{18}O$ values near −30‰ show that these samples are relatively uniform with only small (1–10 μm) Si and Ca-rich patches.

5. Discussion

5.1. Alteration and $\delta^{18}O$ values of uraninite

There is overwhelming evidence from unconformity-type uranium deposits in the Athabasca Basin that

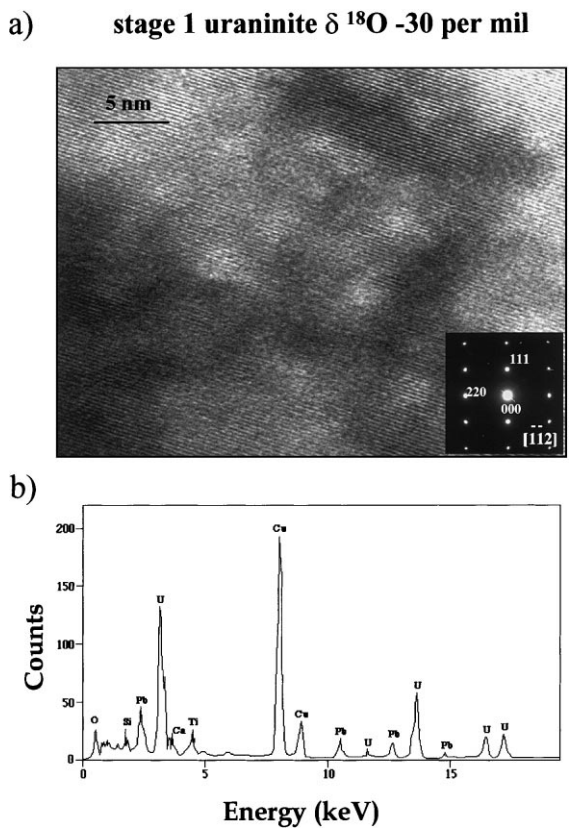

Fig. 3. (a) High resolution transmission electron microscopy (HRTEM) image of primary stage 1 uraninite with a $\delta^{18}O$ value near $-30‰$ with selected area diffraction pattern (inset) showing very few defects (Sample CS 615A1 220-435.15-435.40); (b) Energy dispersive X-ray spectrum (EDS) of stage 1 uraninite with a $\delta^{18}O$ value near $-30‰$ (Sample CS 615A1 220-435.15-435.40). The Cu is from the Cu grid.

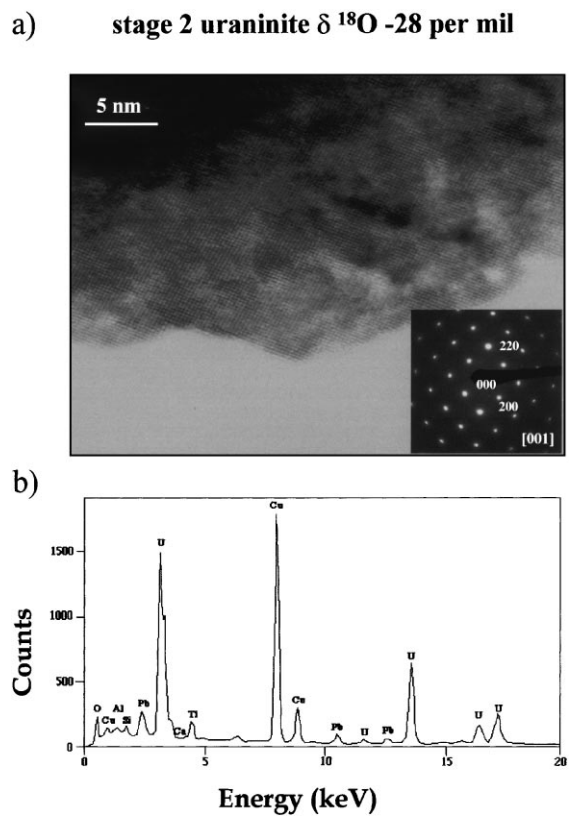

Fig. 4. (a) HRTEM image of primary stage 2 uraninite with a $\delta^{18}O$ value near $-28‰$ with selected area diffraction pattern (inset) showing very few defects (Sample CS 615B2 220-435.15-435.40); (b) Energy dispersive X-ray spectrum (EDS) of stage 2 uraninite with a $\delta^{18}O$ value near $-28‰$ (Sample CS 615B2 220-435.15-435.40). The Cu is from the Cu grid.

primary uraninite was altered by fluids which remobilized lead and uranium, and which altered the uraninite to coffinite and Ca-rich uranyl oxide hydrate minerals [5,6,9,23,29]. In addition, there is a positive correlation between $\delta^{18}O$ values and the SiO_2 and CaO contents of stages 1, 2 and 3 uraninite, Ca-uranyl oxide hydrate minerals, and coffinite, as is expected from the incorporation of relatively ^{18}O-rich SiO_2 and CaO during formation or alteration of uranium minerals [6,8]. Primary stages 1 and 2 uraninite from these deposits have similar chemical compositions, but have $\delta^{18}O$ values that range from $-32‰$ to $-15‰$ [6,9]. However, HRTEM analyses show that primary uraninite that has a $\delta^{18}O$ value near $-18‰$ has higher Si and Ca contents relative to primary uraninite with a $\delta^{18}O$ value near $-30‰$. Therefore, incipient alteration of stages 1 and 2 uraninite occurs on a micro-scale as revealed by HRTEM.

5.2. Radiation effects and oxygen isotope systematics in uraninite

The major source of radiation damage in uraninite results from α-decay of uranium (^{238}U, ^{235}U, and radionuclides in their decay series) although damage sources may include fission fragments and neutrons. Theα-event results in the formation of a high-energy alpha particle (4–5.5 MeV) with a range of 20 μm and a recoil nucleus (i.e., ^{234}U, 0.1 MeV) with a range of ~ 0.02 μm [30]. The energy of the recoil nucleus is almost entirely lost through elastic collisions with the surrounding atoms, and produces several thousand atomic displacements. The α-particle dissipates most of its energy by electronic excitation. However, at lower velocities, near the end of its track, the α-particle undergoes elastic collisions producing several hundred atomic displacements [30].

Stages 1 and 2 uraninite with $\delta^{18}O$ values near $-30‰$ have U-Pb, Pb-Pb, and U-Pb chemical ages ~ 1400 and

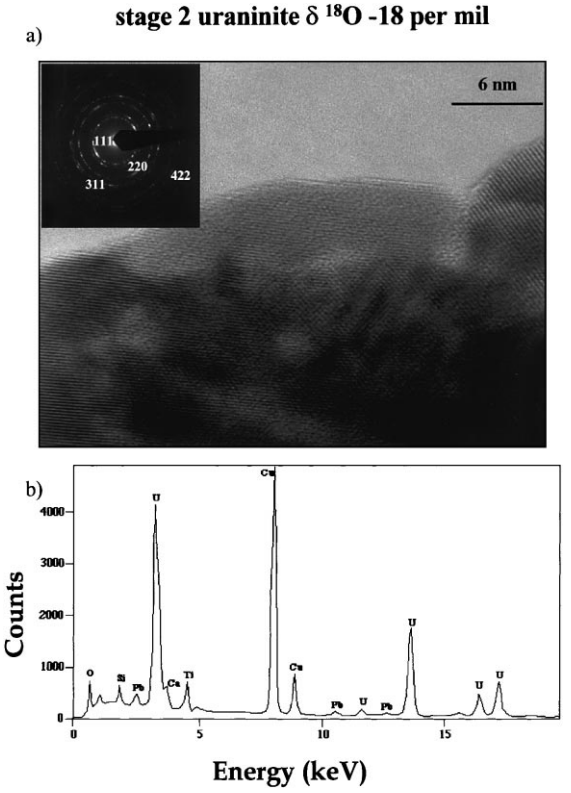

Fig. 5. (a) HRTEM image of primary stage 2 uraninite with a $\delta^{18}O$ value near $-18‰$ with selected area diffraction pattern (inset), showing bent lattice fringes and polycrystalline nature (Sample FH#18 432.30-432.40); (b) Energy dispersive X-ray spectrum (EDS) of stage 2 uraninite with a $\delta^{18}O$ value near $-18‰$ (Sample FH#18 432.30-432.40). The Cu is from the Cu grid.

~ 950 Ma, respectively [5,6,9,23]. These radioactive minerals do not show the development of sub-grains which could have formed from the natural irradiation for over 1000 Ma although their radiation dose is over 500 displacements per atom (dpa). Uraninite has an estimated annealing time for α-recoil tracks of $\sim 15,000$ yr [4]. Therefore, the annealing process in uraninite most likely is efficient enough to remove the very high accumulation of radiation damage, whereas minerals such as zircons typically become metamict (amorphous) at fractions (~ 0.50) of a dpa [31]. However, stage 2 uraninite with $\delta^{18}O$ values near $-18‰$, with relatively higher Si and Ca contents and with U-Pb, Pb-Pb, and U-Pb chemical ages near 1000 Ma [5,9,23], do exhibit sub-grain formation and polygonalization which may be due to the accumulated radiation dose over the past 1000 Ma. The efficiency with which radiation damage is removed by annealing from the structure of uraninite may depend on these chemical impurities. The Si^{4+}–O bond-length is 0.16 nm and can be compared to the U^{4+}–O bond-length of 0.23 nm. Thus, Si^{4+} is generally incompatible with substitution in the structure of uraninite, and Si may stabilize aperiodic regions of damaged structure where various coordination geometries are available, effectively retarding the annealing process. Similar observations are reported for natural monazite, where heavy impurity elements (e.g., Ln, Th, and Pb) retard the annealing process because they are not stable in the monazite structure-type [32]. Alternatively, the sub-grains may have formed during late stage alteration of the uraninite, when Si and Ca were added to the uraninite structure. If true, this alteration occurred within the last 15 000 yr (i.e., the time required to anneal α-recoil tracks in uraninite). However, detailed U-series analyses of these minerals is required to resolve this issue.

Radiation damage accelerates the dissolution of uraninite [3,4,33] and can cause isotope fractionation. Ground waters commonly leach ^{234}U in preference to ^{238}U because the ^{234}U recoil nucleus is located within α-recoil tracks produced by the decay of ^{238}U [4]. Therefore, ^{234}U is readily fractionated from ^{238}U. However, radiation damage will not likely affect the oxygen isotope systematics in uraninite because there is no evidence that ^{18}O will preferentially reside in α-recoil tracks relative to ^{16}O. Therefore, radiation damage will not enhance oxygen isotope fractionation in uraninite.

6. Conclusions

Primary stages 1 and 2 uraninite with low and high $\delta^{18}O$ values (-30 and $-18‰$) from the Cigar Lake unconformity-type uranium deposit were examined by HRTEM. Although the $\delta^{18}O$ values suggest that stages 1 and 2 uraninite interacted with late meteoric waters, stages 1 and 2 uraninite with the lowest $\delta^{18}O$ values are crystalline, essentially defect-free, and chemically homogenous with high Pb and low Si and Ca contents. These radioactive minerals do not show extensive radiation damage such as sub-grain formation or polygonalization, although their radiation dose is over 500 dpa, and therefore the damage must rapidly anneal. In contrast, stage 2 uraninite with a $\delta^{18}O$ value near $-18‰$ is polycrystalline and disordered, and is characterized by relatively high Si and Ca and variable Pb contents. Sub-grain formation and polygonalization of this radioactive mineral may have been caused by the α-decay irradiation dose which accumulated over the past 1000 Ma. The relatively high Si and Ca contents may not have allowed the annealing process to occur uniformly and efficiently. Therefore, the sub-grains and polycrystalline nature of these grains were preserved. Alternatively, the sub-grains formed during the alteration of these uraninite

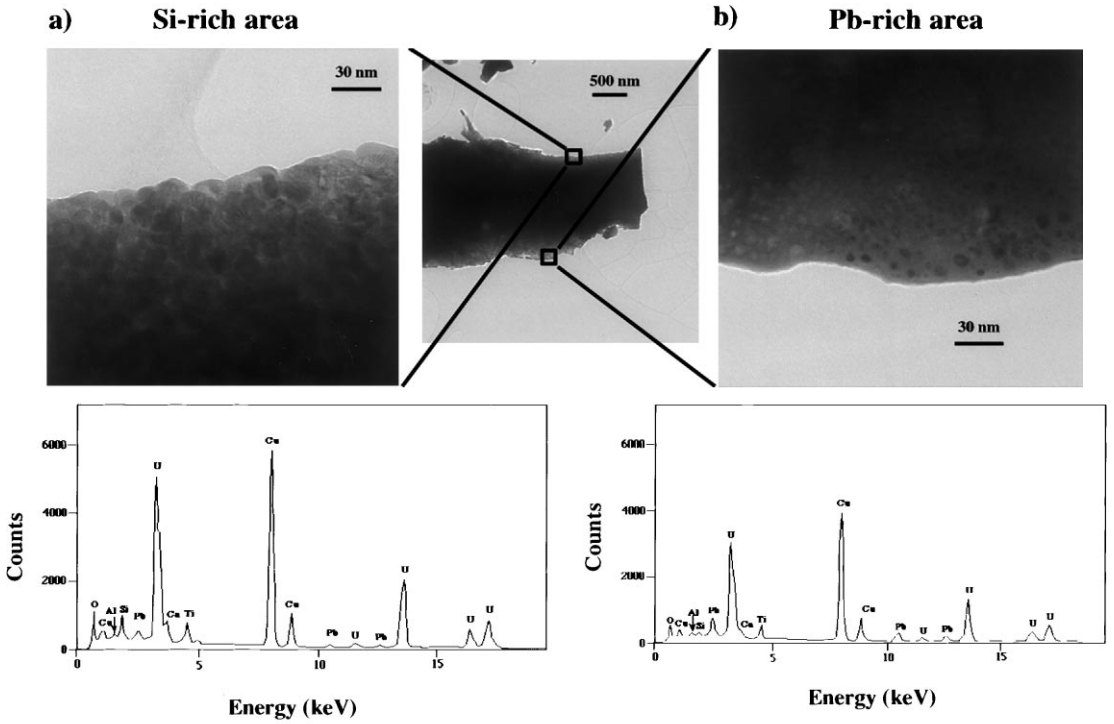

Fig. 6. Bright field image of a chemically hetrogenous stage 2 uraninite with a $\delta^{18}O$ value near $-18‰$ showing: (a) Si-rich area with energy dispersive X-ray spectra (below) and (b) Pb-rich area with energy dispersive X-ray spectrum (below) (Sample FH#18 432.30-432.40). The Cu is from the Cu grid.

grains, within the last 15,000 yr, when Si and Ca were added to the uraninite structure.

The positive correlation between $\delta^{18}O$ values and Si and Ca contents of primary stages 1 and 2 uraninite suggests that incipient alteration of stages 1 and 2 uraninite occurs on a micro-scale and was only detected by HRTEM. In addition, radiation damage effects likely do not affect the oxygen isotope systematics in uraninite. Therefore, stages 1 and 2 uraninite with the lowest $\delta^{18}O$ values most likely retained their original oxygen isotopic composition.

Acknowledgements

The Natural Sciences and Engineering Research Council of Canada (NSERC) supported this work with a Post-Doctoral Fellowship to M.F. This work was also partially supported by Atomic Energy of Canada Ltd. (M.F.) and Basic Energy Science DOE grant DE-FG03-93ER45498. Samples in this study were generously provided by J.J. Cramer (Atomic Energy of Canada LTD.) and David Curtis (Los Alamos National Laboratory). This manuscript has benefited from the reviewer's comments.

References

[1] R.J. Finch, R.C. Ewing, J. Nucl. Mater. 190 (1992) 133.
[2] J. Janeczek, R.C. Ewing, V.M. Oversby, L.O. Werme, J. Nucl. Mater. 238 (1996) 121.
[3] R.L. Fleischer, Geochim. Cosmochim 46 (1982) 2191.
[4] Y. Eyal, R.L. Fleischer, Nature 314 (1985) 519.
[5] M. Fayek, J. Janeczek, P.C. Ewing, Appl. Geochem. 12 (1997) 549.
[6] M. Fayek, T.K. Kyser, Can. Miner. 35 (1997) 627.
[7] J. Janeczek, R.C. Ewing, J. Nucl. Mater. 190 (1992) 157.
[8] T.G. Kotzer, T.K. Kyser, in: Y. Kharaka, A. Maest (Eds.), Proceedings of the Seventh International Symposium on Water–Rock Interaction, Park City, Utah, July 13–18, 1992, p. 1177.
[9] T.G. Kotzer, T.K. Kyser, Am. Mineral. 78 (1993) 1262.
[10] K. Hattori, S. Halas, Geochim. Cosmochim. Acta 46 (1982) 1863.
[11] Y. Zheng, Geochim. Cosmochim. Acta. 55 (1991) 2299.
[12] M. Fayek, T.K. Kyser, Geochim. Cosmochim. Acta. (accepted) (1999).
[13] T.G. Kotzer, T.K. Kyser, Summary of investigations 1990: Sask. energy and mines, Sask. Geol. Surv. Misc. Rep. 90-4 (1990) 153.
[14] S.B. Romberger, Uranium Geochemistry, Resources, Institution of Mining and Metallurgy, 1985, p. 12.
[15] J.J. Cramer, AECL Rep. 11204 (1995) 32.

[16] J. Janeczek, R.C. Ewing, V.M. Oversby, L.O. Werme, J. Nucl. Mater. 238 (1996) 121.
[17] P. Ramaekers, C.D. Dunn, Sask. Geol. Soc. Spec. Pub. 3 (1977) 297.
[18] P. Ramaekers, Proterozoic Basins of Canada in: F.H.A. Campbell (Ed.), Geol. Surv. Can. Paper 81–10, 1981, p. 219.
[19] J.F. Lewry, T.I.I. Sibbald, Can. J. Earth Sci. 14 (1977) 1453.
[20] J.F. Lewry, T.I.I. Sibbald, Tectonophysics 68 (1980) 45.
[21] J.F. Lewry, T.I.I. Sibbald, D.C.P. Scheledewitz, in: L.D. Ayers, P.C. Thurston, K.D. Card, W. Weber (Eds.), Evolution of Archean Supracrustal Sequences, GAC, Special Paper 28, 1985, p. 239.
[22] R. Macdonald, Summary of investigations, Sask. Energy and Mines, Sask. Geol. Surv. Misc. Rep. 87-4 (1987) 87.
[23] T.G. Kotzer, T.K. Kyser, Chem. Geol. 120 (1995) 45.
[24] J. Hoeve, T.I.I. Sibbald, P. Ramaekers, J.F. Lewry, in: S. Fergusom, A. Goleby (Eds.), Uranium in the Pine Creek Geosyncline, Vienna, Int. Atomic Energy Agency, 1980, p. 575.
[25] R. Wallis, N. Saracoglu, J. Brummer, J. Golightly, Geol. Surv. Canada Paper 82-11 (1983) 71.
[26] J. Marlatt, B. McGill, R. Matthews, V. Sopuck, G. Pollock, in: I.A. Homeniuk (Ed.), The Geological Society of CIM First Annual Field Conference, 1992, p. 118.
[27] R. Clayton, T.K. Mayeda, Geochim. Cosmochim. Acta. 27 (1963) 43.
[28] P. Baertschi, Earth Planet. Sci. Lett. 31 (1976) 341.
[29] G.L. Cumming, D. Krstic, Can. J. Earth Sci. 29 (1992) 1623.
[30] R.C. Ewing, W.J. Weber, F.W. Clinard Jr., Progr. Nucl. Energy 29 (2) 1995, p. 63.
[31] W.J. Weber, R.C. Ewing, L.-M. Wang, J. Mater. Res. 9 (3) (1994) 688.
[32] A. Meldrum, L.A. Boatner, L.-M. Wang, R.C. Ewing, Mater. Res. Soc. Symp. Proc. 427, 1996.
[33] R.L. Fleischer, Science 207 (1980) 979.
[34] J. Hoeve, T.I.I. Sibbald, Econ. Geol. 73 (1978) 1450.